

P O L S K A A K A D E M I A N A U K

I N S T Y T U T M A S Z Y N P R Z E P Ł Y W O W Y C H

**TRANSACTIONS
OF THE INSTITUTE OF
FLUID-FLOW MACHINERY**

PRACE

I N S T Y T U T U M A S Z Y N P R Z E P Ł Y W O W Y C H

104



GDAŃSK 1998

THE TRANSACTIONS OF THE INSTITUTE OF FLUID-FLOW MACHINERY

exist for the publication of theoretical and experimental investigations of all aspects of the mechanics and thermodynamics of fluid-flow with special reference to fluid-flow machines

*

PRACE INSTYTUTU MASZYN PRZEPIYWOWYCH

poświęcone są publikacjom naukowym z zakresu teorii i badań doświadczalnych w dziedzinie mechaniki i termodynamiki przepływów, ze szczególnym uwzględnieniem problematyki maszyn przepływowych

Wydanie publikacji zostało dofinansowane przez PAN ze środków DOT uzyskanych z Komitetu Badań Naukowych


EDITORIAL BOARD – RADA REDAKCYJNA

ZBIGNIEW BILICKI * TADEUSZ GERLACH * HENRYK JARZYNA
JAN KICIŃSKI * JERZY KRZYŻANOWSKI (CHAIRMAN – PRZEWODNICZĄCY)
WOJCIECH PIETRASZKIEWICZ * WŁODZIMIERZ J. PROSNAK
JÓZEF ŚMIGIELSKI * ZENON ZAKRZEWSKI

EDITORIAL COMMITTEE – KOMITET REDAKCYJNY

EUSTACHY S. BURKA (EDITOR-IN-CHIEF – REDAKTOR NACZELNY)
JAROSŁAW MIKIELEWICZ
EDWARD ŚLIWICKI (EXECUTIVE EDITOR – REDAKTOR) * ANDRZEJ ŻABICKI

EDITORIAL OFFICE – REDAKCJA

Wydawnictwo Instytutu Maszyn Przepływowych
Polskiej Akademii Nauk
ul. Gen. Józefa Fiszer 14, 80-952 Gdańsk, skr. poczt. 621,
 (0-58) 341-12-71 wew. 141, fax: (0-58) 341-61-44,
e-mail: esli@imppan.imp.pg.gda.pl

ISSN 0079-3205

ALEXANDER R. JUNG¹, JÜRGEN F. MAYER¹ and HEINZ STETTER¹

Unsteady blade loads caused by stator/rotor interaction in an axial turbine stage

The results of a simulation of the three-dimensional unsteady viscous flow in a highly loaded last stage of an axial flow low pressure turbine are presented. The focus in the flow analysis is on the temporal fluctuations of the rotor lift and the resulting unsteady forces and torques acting on the rotor blading. In the lower 50 % of the rotor span the stator exit flow is transonic and strong interaction effects between the stator and the rotor potentials can be observed. The resulting temporal fluctuations of the static pressure on the rotor blades amount to a maximum of more than 40 % of the time-mean value. In the region between 20 and 40 % of the span where the unsteady interaction effects are maximal, complex shock motion patterns are found. The unsteady static pressure is integrated along the chord and over the surface of the rotor blade to yield the unsteady distributed loads, forces, and torques, respectively. These quantities are analysed both in time and the frequency domain. It is found that the first harmonic of the blade passing frequency of the driving torque amounts to 6.3 % of the time-mean value. The second harmonic still amounts to 3.4 %.

1. Introduction

In the present design process of a turbomachine, numerical methods play a major role with constantly increasing importance. At the various stages of new blade development, different modelling techniques are used ranging from very efficient one-dimensional through flow codes for the estimation of the very basics of the flow characteristics up to three-dimensional steady-state Navier-Stokes solvers for the fine tuning of the blade design in multistage turbomachinery. Various types of 3D methods are employed. Due to the still high computational costs, however, simulations of the unsteady viscous three-dimensional flow field have not yet been established as a standard means in the industrial blade design process.

Consideration of unsteady effects in turbomachinery stage flow can, on one hand, be beneficial for the development of more efficient turbomachinery stages even without having to analyse the time history of flow but rather looking at averaged quantities. Some publications indicate, for example, that the rotor exit flow

¹Institut für Thermische Strömungsmaschinen und Maschinenlaboratorium, University of Stuttgart, Germany

angle can be predicted much more accurately from the time-averaged unsteady flow field than from that of a steady-state simulation, in which unsteady effects are insufficiently or not at all taken into account, see e.g. Gallus et al. (1994), Jung et al. (1996). Time-dependent phenomena like unsteady shock and vortex motion, vortex shedding, and blade-row interaction effects may have a strong influence on the time-averaged flow field. Generally, steady-state computations cannot describe these phenomena and therefore the results may differ significantly from the time-averaged results of unsteady simulations. A periodically moving shock on an airfoil, for example, will show as a smeared pressure wave in its time-averaged flow field, whereas a steady-state simulation will show the shock at some fixed location with a different gradient and a different inclination. Thus, static pressure distributions as well as blade shapes optimized with respect to those distributions might look considerably different for both simulation methods.

On the other hand, the analysis of the time-dependent flow field helps to improve our understanding of the flow physics in turbomachines with respect to unsteady loss production mechanisms, forced blade vibration, flutter, and shock boundary layer interaction for example. The latter examples are especially important in structural dynamics considerations as unsteady blade forces can lead to complete blade failure. It is therefore crucial to accurately predict unsteady forces and torques in order to prevent that worst case from happen. Most of the scientists in unsteady aerodynamics analyse the blade lift fluctuations and unsteady pressure amplitudes, see e.g. Arnone and Pacciani (1995), Madavan et al. (1993). There is however little information on the integral effect of these fluctuations on the blading. This might be due to the geometry of the test cases, as most of the turbomachines under consideration have rather massive blades and moderate aspect ratios such that blade vibrations caused by unsteady forces are not of primary concern. Another reason might be that there are hardly any experimental data available which deal with high-frequency stresses or strains of rotor bladings with which the results can be compared.

The aim of this paper is to evaluate and describe the unsteady fluctuations of the rotor blade loads which are caused by the potential interaction effects of the stator exit flow with the rotor flow. This analysis is performed in order to get a feeling of the magnitude of this quantities and to determine whether or not they have to be taken into account in structural dynamics or high cycle fatigue considerations.

The turbine stage considered here is the highly loaded last stage of a transonic axial flow turbine with very long and strongly twisted blades. In earlier publications the steady-state, the time-averaged, and the unsteady flow field was presented and comparison with steady-state experimental data was made, Merz et al. (1995), Jung et al. (1996), Stetter et al. (1996). The results show that in the transonic region of the stator exit flow the unsteady fluctuations have a considerable impact on the instantaneous blade loads and driving torques of the individual rotor blades. The analysis is performed in the time domain as well as in the frequency domain.

2. Turbine geometry and spatial discretization

The stage consists of 44 stator blades and 60 rotor blades. Due to the long blades the Mach numbers associated with the rotational speed of 12,600 rpm varies from about 0.6 at the hub to about 1.4 near the casing. Thus, together with the strong twisting of the blades, the operating conditions lead to a highly unsteady and three-dimensional flow.

Due to the rather large pitch ratio of 1.364, the stability limitation that comes along with the time-inclination method is violated such that a single passage calculation cannot be performed successfully. The extension of the computational domain to 2 stator and 3 rotor passages brings the pitch ratio closer to 1, that is to say $(2 \cdot 60)/(3 \cdot 44) = 0.909$, and a stable calculation can be carried out because now the amount of necessary inclination of the time axis for the extended stator and rotor domain, respectively, is much less than in the single passage case. It should be noted that also for the extended domain, the method allows the modelling of the exact pitch ratio and no approximation needs to be made in this respect. Each stator passage was discretized with 92,169 nodes, the rotor passages were discretized with 156,585 nodes each, and the rotor tip gap regions consisted of 18,690 nodes each, yielding a total of 0.71 million grid points for the whole computational domain. An perspective view of the turbine showing the grid at the hub and on the blade surfaces is shown in Fig. 1.

3. Numerical method

The equations solved are the fully three-dimensional, unsteady, Favre-averaged Navier-Stokes equations. The set of equations is written for a cylindrical coordinate system that rotates at constant angular velocity, see Jung et al. (1996). The fluid is assumed to behave as an ideal gas with a constant ratio of specific heat capacities. A modified algebraic Baldwin-Lomax model is used to describe the effects of turbulence. The governing equations are discretized in space in finite volume form on curved hexahedral control volumes. The state variables are located at the vertices of each cell and a piece wise linear variation over the cell faces between the vertices is assumed. The method to evaluate the convective and diffusive residuals of each control volume and to add artificial diffusion in order to prevent odd-even decoupling and to control shock capturing is based on the work of Jameson et al. (1981). The net flux imbalance for each control volume is used to update the flow variables through an explicit five-stage Jameson-type Runge-Kutta time stepping scheme.

In cases of unsteady simulations in which the stator blade count is different from the rotor blade count, a time-inclining method for three dimensions based on the work of Giles (1991) is used in order to model the exact ratio of the blade counts. In this approach, time-transformations are applied to both the stator and the rotor domains and different time steps are used in these domains. In this

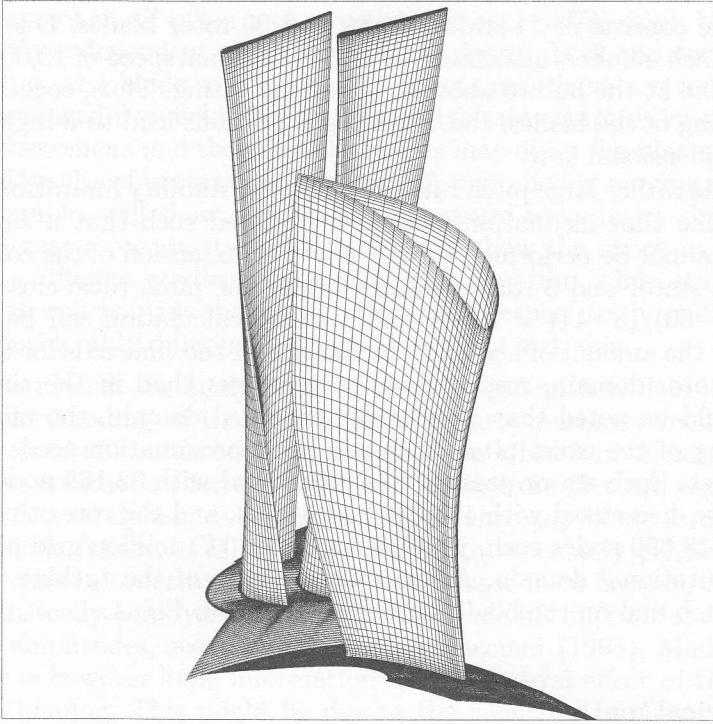


Fig. 1. Perspective view of the computational grid for the turbine stage.

way simple periodicity conditions can be applied at the boundaries in pitch-wise direction although these boundaries are not periodic in the physical domain. Multiple blade passages can be used to overcome the stability limitation of the time-inclination method for the cases in which the difference in the blade counts of the stage is so large that in the time-transformed space the principle of causality would be violated.

At the inlet and exit boundaries as well as at boundaries between two domains in the case of steady-state flow interaction of two blade rows, a non-reflecting post-correction method based on the work of Giles (1988) is applied to prevent spurious reflections from waves that leave the computational domain. Solid surfaces are assumed adiabatic and the no-slip condition is applied. Periodicity in pitch-wise direction is ensured through the use of dummy cells that keep copies of the periodic values such that the points on these boundaries can be treated like interior points.

Block-structured H-type grids which consist of curved hexahedral cells and which are fixed in the relative frame of reference are used in a multiblock topology in order to allow easy modelling of blade gaps as well as of computational

domains which consist of multiple blade passages. At the sliding interfaces between stationary and rotating blade rows the grids are overlapped by one grid cell. An interpolation procedure consistent with the second order spatial accuracy of the numerical scheme is used to interchange the flow variables at every time step of the integration procedure. As the rotor grid moves relative to the stator, the rotation of the rotor is integrated in time in order to track the position of the grid blocks for a time-resolved coupling at the interface region.

For steady-state calculations a full multigrid method as well as local time stepping and implicit residual smoothing with variable coefficients can be used to accelerate convergence to a very large extent, see Merz et al. (1995). In the case of unsteady calculations a time-consistent multigrid scheme based on the work of He (1996), an implicit residual averaging method for global time steps, or an implicit time-accurate dual time-stepping method (see Jameson (1991)) which solves the governing equations via an explicit time-integration in a pseudo time and which allows the use of all the acceleration methods that apply to steady state simulations can be used to efficiently accelerate the solution process. Additionally, the solver is parallelized based on the multiblock structure of the spatial discretization using the message passing interface (MPI). The code can be run efficiently on single-processor computers, workstation clusters, and parallel computers. Vector or parallel-vector supercomputers are also applicative as for the CPU-time consuming kernel routines the ratio of vector operations versus scalar operations is greater than 97 %.

4. Results

A steady-state simulation was carried out in order to get the initial data for the unsteady calculation. The time-consistent multigrid method was used to accelerate the solution process. Each domain passing period, i. e. the time it takes for all three passages of the rotor domain to pass a stator blade, was calculated with 1400 explicit integration steps. The memory requirement was about 110 MBytes. Each of the time-steps took about 80 seconds of CPU time on a 333 MHz DEC Alpha workstation. Due to the skewed cells in the upper region of the span, the CFL number had to be reduced to a value of 1.3 in order to perform a stable integration. This is a rather small value compared to the theoretical value of 4.0 of the five-stage Runge-Kutta scheme. Up to four multigrid levels had to be used to account for the relatively large time-step value which is far beyond the stability limit in the viscous regions near solid walls and in the tip gap. The efficiency of the so accelerated calculation was about 6 times higher than that of the unaccelerated scheme. The mass flow rate in the simulation amounted to 4.82 kg/s and was slightly lower than the experimentally obtained mass flow rate of 4.87 kg/s. This mass flow defect might be due to numerical losses caused by the relatively coarse discretization.

4.1. Unsteady Mach number distribution

The diagrams in Figs. 2 and 3 show absolute Mach number contours for an azimuthal cut at about 33% of the span at eight instants in time during one blade passing period. Time increases in clockwise direction. The increment of the contour lines is 0.01 for Fig. 2 and 0.02 for Fig. 3, respectively. The sonic line is plotted with dashes and can be seen in the blade-to-blade passages of the stator and the rotor. The whole region between these lines - with the exception of the boundary layers and the interior of the stator wakes, of course - is supersonic in the absolute frame of reference but subsonic in the relative frame. The different contour line densities in the two figures have been chosen to point out two distinct phenomena. Fig. 2 shows the instantaneous flow field for a few adjacent blade passages from the inlet to the exit boundary. From the diagrams in this figure it can be observed how the velocity gradients which are caused by the rather weak stator trailing edge shock interact with the potential effect caused by the rotor blades and with the rotor blades themselves. Depending on the instantaneous position of the airfoils in the two blade rows relative to each other, very complex flow patterns are formed which are dominated by the interaction of the impingements, deflections, and reflections of the velocity gradients and the corresponding waves. The deflections whose orientations are almost orthogonal to that of the shock waves appear to have a more or less stationary position, whereas the positions and shapes of the shock waves change constantly. These deflections allow in fact to identify the stator pitch from the flow pattern even downstream of the rotor blades leading edges. As another effect caused by the strong unsteady fluctuations in the flow it can be observed how the rotor wakes oscillate with twice the blade passing frequency and how pieces of the wakes are shed with every oscillation cycle.

The diagrams in Fig. 3 show an enlargement of the gap region between the stator and the rotor blades at the same position of the span. The density of the isolines in these plots was chosen lower than in Fig. 2. In the interior of the stator wakes, the sonic lines can be identified. The pressure waves emerging from the stator blades trailing edges cross the wakes and prevent them from growing larger. Following the motion of the sonic line in the wakes, it can be observed how the wake grows and narrows near its downstream end until a vortex-like piece of subsonic wake is carried along, accelerated, and convected downstream. This process recurs three times during each blade passing period.

4.2. Blade pressure fluctuations

Due to the long and strongly twisted blades, the flow in the turbine stage is highly three-dimensional. The characteristics of the flow varies considerably along the span. In the transonic region strong blade row interaction effects can be observed which are mainly of inviscid nature, i. e. potential interaction, whereas in the region above 50% of the span where the stator exit flow is subsonic hardly any potential interaction takes place at all. Figs. 4 to 7 depict the unsteady rotor

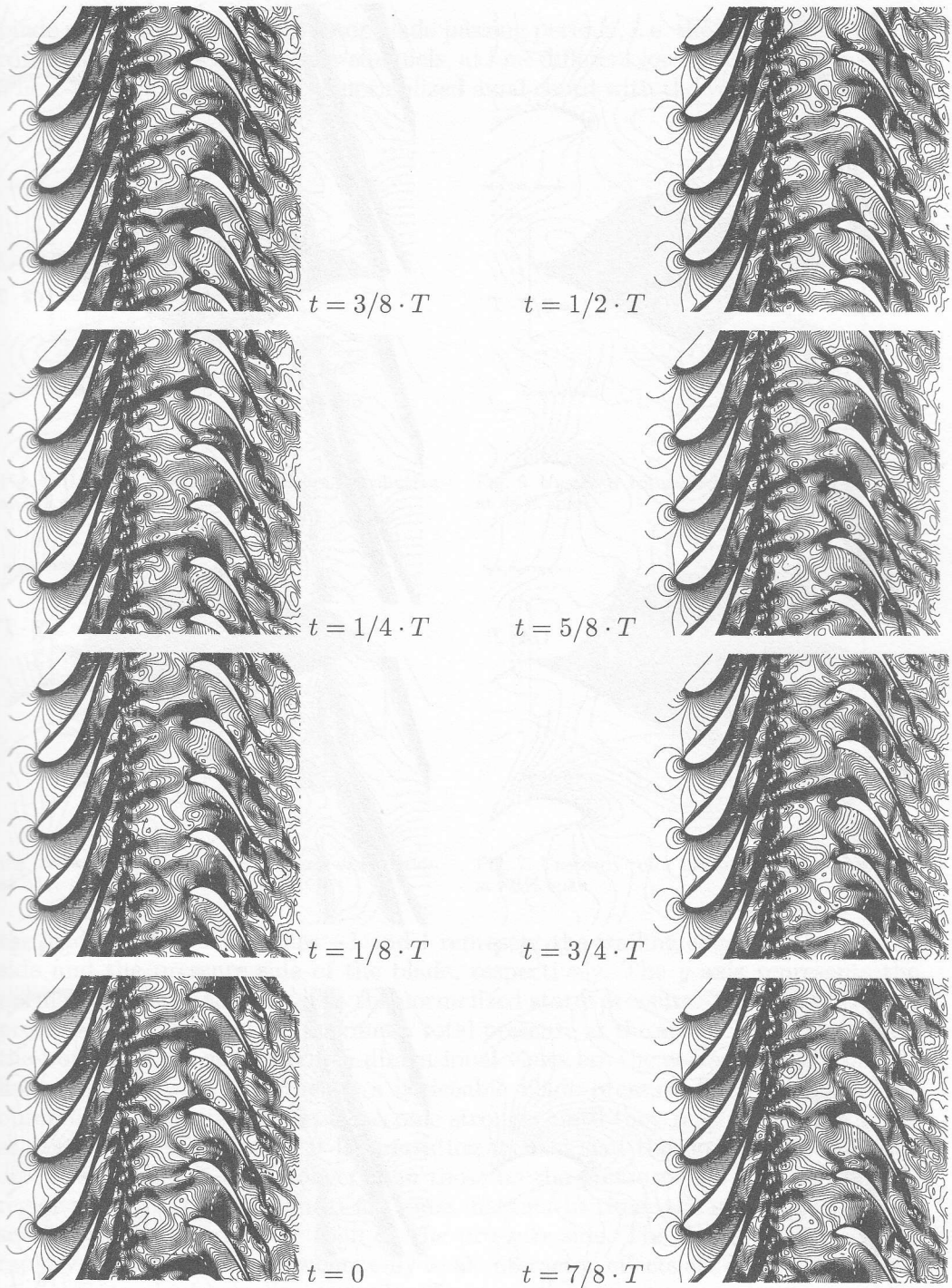


Fig. 2. Instantaneous absolute Mach number contours at 33% span during one blade passing period T .

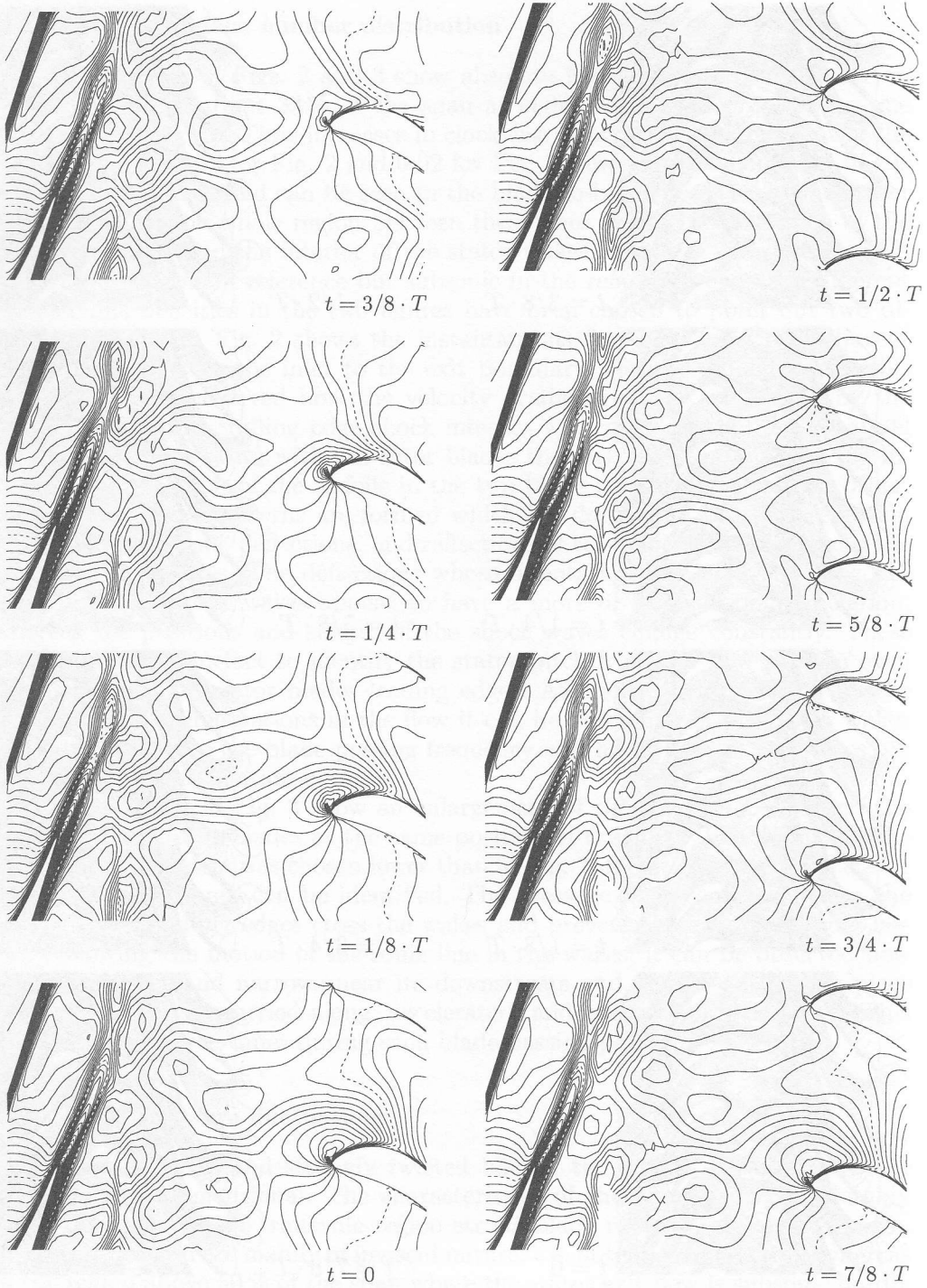


Fig. 3. Mach number contours in the axial gap between the stator blade row and the rotor blade row at 33% span during one blade passing period.

blade pressure during three rotor blade passing periods, i. e. the time it takes for a rotor blade to pass three stator channels, at four different locations along the span. The x -axis corresponds to the normalized axial chord with the value zero being at

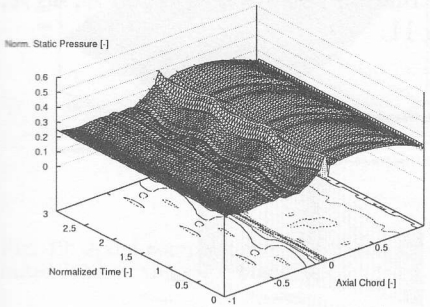


Fig. 4. Unsteady rotor blade pressure distribution at 4% span.

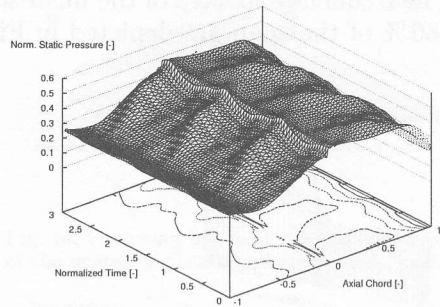


Fig. 6. Unsteady rotor blade pressure distribution at 48% span.

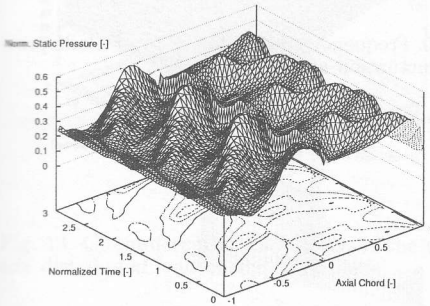


Fig. 5. Unsteady rotor blade pressure distribution at 33% span.

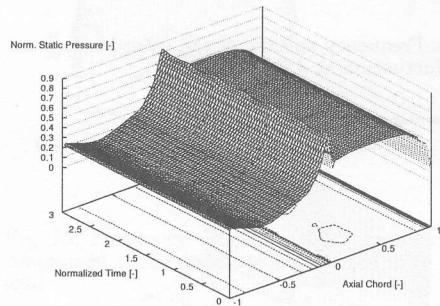


Fig. 7. Unsteady rotor blade pressure distribution at 86% span.

the leading edge. The values -1 and 1 represent the trailing edges on the suction side and the pressure side of the blade, respectively. The y -axis represents the normalized time and the z -axis the normalized static pressure. The normalization pressure is taken to be the maximum total pressure at the stator inlet. Plotted on the bottom plane of these three-dimensional views are the corresponding contour lines. Already at 4% of the span noticeable blade pressure fluctuations can be observed. The unsteady effects become stronger until they reach their maximum at about 33% of the span. It is interesting to note that the pressure fluctuations on the suction side are stronger than those on the pressure side such that in the region of highest unsteadiness for some instants in time, the static pressure on suction side is even higher than on the pressure side. The fluctuations decrease rapidly towards mid-span, where only weak interaction effects are observable. From mid-span to the blade tip unsteady effects with respect to pressure fluctuations are negligible. This is a consequence of the high circumferential component of the

flow velocity together with the rather wide axial gap between the blade rows in this region as the flow particles that leave the stator blade passage have to cross almost half of the annulus before they enter the rotor passage. Thus there is plenty of time for the flow to mix out and calm.

The frequency spectra of the unsteady rotor blade pressure at 4 %, 33 %, 48 %, and 86 % of the span are depicted in Figs. 8 to 11.

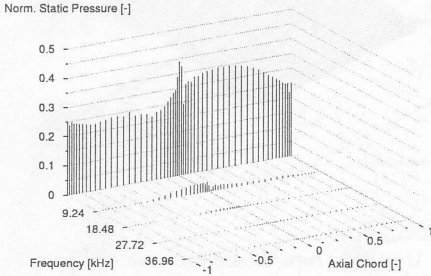


Fig. 8. Frequency spectra of the rotor blade pressure fluctuation at 4 % span.

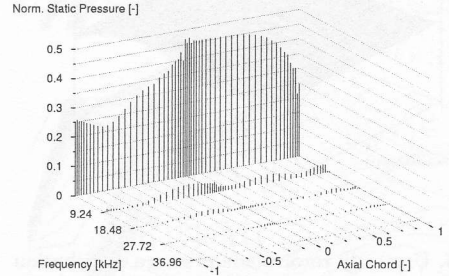


Fig. 10. Frequency spectra of the rotor blade pressure fluctuation at 48 % span.

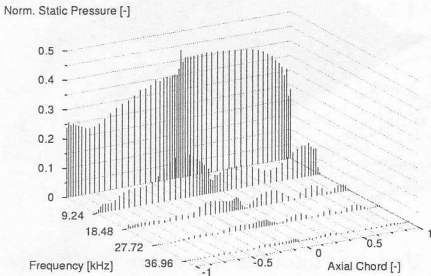


Fig. 9. Frequency spectra of the rotor blade pressure fluctuation at 33 % span.

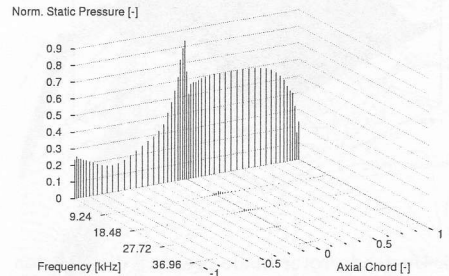


Fig. 11. Frequency spectra of the rotor blade pressure fluctuation at 86 % span.

Here, the y -axis represents the frequency as harmonics of the rotor blade passing frequency, i. e. multiples of the rotational speed times the stator blade count. The zeroth order harmonic corresponds to the time-mean pressure. It can be seen from these plots that in those regions of the rotor blading where there is only weak unsteadiness, i. e. very close to the hub and from about mid-span towards the casing, the predominant contribution to the unsteadiness comes from the first harmonic. It affects mainly the suction side of the blade from the leading edge to about mid-chord. This can be explained with the periodic interaction of the potential fields of the stator and the rotor. Even close to the casing at 86 % of the span a very weak potential interaction can be observed.

In the transonic flow region the frequency characteristics of the blade pressure

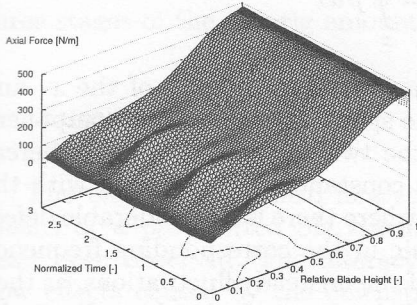


Fig. 12. Axial component of the unsteady distributed load on the rotor blade.

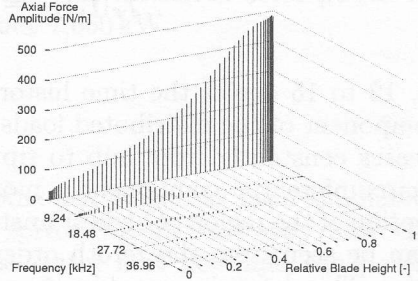


Fig. 14. Frequency spectra of the axial component of the unsteady distributed rotor blade load.

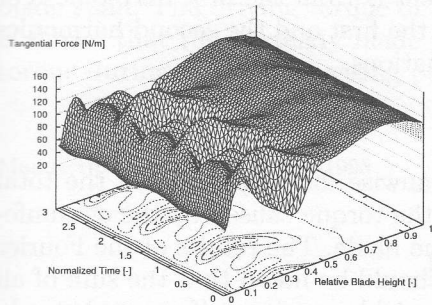


Fig. 13. Circumferential component of the unsteady distributed load on the rotor blade.

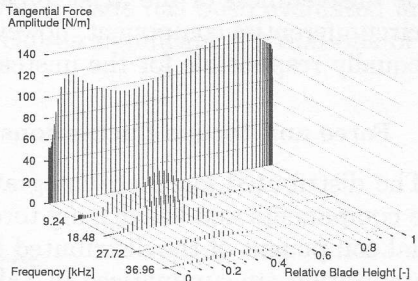


Fig. 15. Frequency spectra of the circumferential component of the unsteady distributed rotor blade load.

fluctuations look different, see Fig. 9. Here the amplitudes of the first harmonic amount to a maximum value of over 40 % of the time-mean value at about 25 % axial chord of the suction side and more than 30 % of the time-mean on the pressure side near the trailing edge at about 90 % axial chord. The second and third harmonics also add considerably to the unsteady blade lift. The contributions of the fourth and higher order harmonics of the blade passing frequency turn out to be insignificant.

4.3. Unsteady blade loads

In order to evaluate the unsteady loads on the rotor blades, the blade pressure fluctuations are integrated along the blade chord to yield the axial component (index x) and the circumferential component (index φ) of the distributed loads dependent on both time and spanwise location:

$$f_x(r, t) = \frac{\partial}{\partial r} F_x = \oint_{\varphi} p d\varphi$$

$$f_{\varphi}(r, t) = \frac{\partial}{\partial r} F_{\varphi} = \oint_x p dx$$

Figs. 12 to 15 depict the time history and the frequency spectra of the x - and φ -component of the distributed loads along the span. The axial force component increases constantly from hub to tip due to the twisting of the blades whereas the circumferential component is more or less constant along the span with the exception of the region of highest unsteadiness where there is a considerable defect as can be seen from the zeroth order harmonic in the corresponding frequency spectra. This defect is caused by the presence of the unsteady fluctuations, as they reduce the time-mean load due to their inter-blade phase relationships. From the time history it is very obvious that there is hardly any unsteadiness in the upper half of the blade span. It is worthwhile to note that the by far largest contribution to the unsteadiness of the axial force component is from the first harmonic. For the circumferential component, however, both the first and the second harmonics are equally responsible for the unsteady fluctuations.

4.4. Force and torque fluctuations

The distributed loads are integrated in spanwise direction to yield the total force components and the driving torque, i. e. the torque caused by the circumferential component of the distributed load of one blade. The results of the Fourier decomposition are summarized in Table 1. It should be noted that the sum of all the torques of the individual blades, of course, yields a quite uniform and steady global torque at the engine shaft as due to the relationships of the inter-blade phase angles of the individual torques the unsteadiness is averaged out over the whole annulus; the unsteady portion of the torque of the single blade, however, is nonetheless interesting to evaluate in order get a feeling for its order of magnitude.

Table 1. Amplitudes of the first three harmonics of the blade passing frequency of the axial and circumferential forces and the driving torque, normalized with respect to the corresponding zeroth order harmonic

	Harmonic Order		
	1.	2.	3.
Axial Force	6.69 %	0.72 %	0.28 %
Circumferential Force	7.32 %	4.10 %	0.95 %
Driving Torque	6.27 %	3.38 %	0.81 %

The ratio of the zeroth order harmonics of the axial and circumferential force component is 2.003. The power of the whole stage as calculated from the time-mean value of the driving torque of a single blade amounts to 692 kW which

is a reasonable value since in the experiments the measured total power of all three stages of the test rig amounted to about 1,660 kW.

5. Summary

The unsteady flow field in a steam turbine last stage has been simulated by means of a parallelized 3D Navier-Stokes solver. Strong unsteady flow effects have been observed. The interaction of the stator exit flow and the potential flow effects caused by the downstream rotor blade row are shown by means of a series of contour plots. The computed pressure field has been analysed in the frequency domain; the unsteady blade loads have been evaluated. It is shown that the significant unsteady effects concentrate to the lower half of the rotor blade span. The driving torque of a single rotor blade has been evaluated and it is shown that the unsteady blade pressure causes significant fluctuations of this torque during one blade passing period.

Manuscript received in March 1998

References

- [1] Arnone, A., Pacciani, R., 1995: *Rotor-stator interaction analysis using the Navier-Stokes equations and a multigrid method*, ASME 95-GT-177.
- [2] Gallus, H. E., Zeschky, J., Hah, C., 1994: *Endwall and unsteady phenomena in an axial turbine stage*, ASME 94-GT-143.
- [3] Giles, M. B., 1988: *Non-reflecting boundary conditions for the Euler equations*, Tech. Rep. TR-88-1, MIT CFD Laboratory.
- [4] Giles, M. B., 1991: *UNSFLO: A numerical method for the calculation of unsteady flow in turbomachinery*, GTL Rep. No. 205, MIT Gas Turbine Laboratory.
- [5] He, L., 1996: *Time-marching calculations of unsteady flows, blade row interaction and flutter*, VKI-LS 1996-05.
- [6] Jameson, A., 1991: *Time dependent calculations using multigrid with applications to unsteady flows past airfoils*, AIAA 91-1596.
- [7] Jameson, A., Schmidt, W., Turkel, E., 1981: *Numerical solutions of the Euler equations by finite volume methods using Runge Kutta time-stepping schemes*, AIAA 81-1259.

- [8] Jung, A. R., Mayer, J. F., Stetter, H., 1996: *Simulation of 3D-unsteady stator/rotor interaction in turbomachinery stages of arbitrary pitch ratio*, ASME Paper 96-GT-69.
- [9] Madavan, N. K., Rai, M. M., Gavali, S., 1993: *Multipassage three-dimensional Navier-Stokes simulation of turbine rotor-stator interaction*, *Journal of Propulsion and Power*, vol. 9(3), pp. 389-396.
- [10] Merz, R., Krückels, J., Mayer, J. F., Stetter, H., 1995: *Calculation of three-dimensional viscous transonic turbine stage flow including tip clearance effects*, ASME Paper 95-GT-76.
- [11] Stetter, H., Jung, A. R., Mayer, J. F., 1996: *Numerical studies of unsteady flow phenomena in multi-blade row environment*, in *Aerodynamics of Turbomachinery*, IMechE Seminar Publication 1996-21.

Zmienne obciążenia łopatek wywołane oddziaływaniem stojan-wirnik w stopniu turbiny osiowej

Streszczenie

Przedstawiono wyniki symulacji nieustalonego trójwymiarowego przepływu lepkiego w wysoce obciążonym niskociśnieniowym stopniu turbiny osiowej. W analizie przepływu uwagę skupiono na fluktuacjach chwilowych siły nośnej wirnika oraz wynikających stąd nieustalonych siłach i momentach działających na ułopatkowanie wirnika.